ACS APPLIED MATERIALS & INTERFACES

Research Article

www.acsami.org

Enhanced Light Harvesting in Dye-Sensitized Solar Cells Coupled with Titania Nanotube Photonic Crystals: A Theoretical Study

Min Guo, Zehui Yong, Keyu Xie, Jia Lin, Yu Wang, and Haitao Huang*

Department of Applied Physics and Materials Research Center, The Hong Kong Polytechnic University, Hong Kong, China

ABSTRACT: Herein we present a theoretical analysis on the optical properties and the photocurrent enhancement of nanotube-based dye-sensitized solar cells (DSSCs) coupled with a TiO_2 nanotube (NT) photonic crystal (PC). It is found that the introduction of a TiO_2 nanotube PC produces both Bragg mirror effect and Fabry–Perot cavity behavior, leading to a significant enhancement of light harvesting for photons in the photonic bandgap and at the two band edges. In addition, an increased amount of surface-anchored dye due to the larger surface area in the NT PC layer also causes absorption enhancement in the whole visible spectrum. The effects of structural parameters of the PC, such as the thickness of the PC layer, the axial lattice constant, the diameter of the nanotube, and light incident angle, on the optical properties and photocurrent magnification are thoroughly studied. The optimum structural parameters are proposed, which not only provide guidance but also offer further opportunities in the design and applications of TiO_2 nanotube photonic crystals.

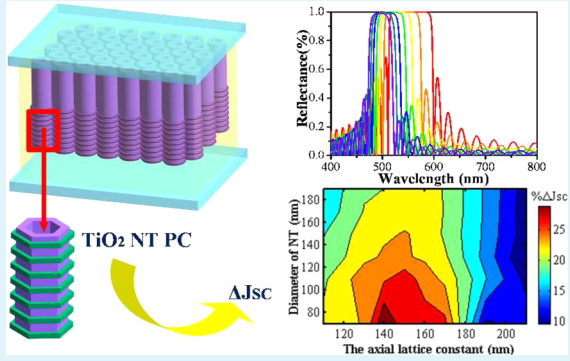

KEYWORDS: *photonic crystal, TiO_2 nanotube, dye-sensitized solar cell, light harvesting, photocurrent, photonic bandgap*

INTRODUCTION

Dye-sensitized solar cells (DSSCs) are considered as an alternative to traditional expensive silicon solar cells, due to their lower material cost, simpler fabrication process, and even lower investment cost.[1−3] The prevailing cell consists of a nanocrystalline TiO_2 layer sensitized by ruthenium dye, which absorbs light and injects photogenerated electrons to the TiO_2 network, and redox electrolyte, which fills in the space interval of the TiO_2 network and electrodes.[4]

Although the record power conversion efficiency of DSSCs has reached 12%,[5] it is still lower than that of silicon-based cells as well as thin film cells, which limits their applications and commercialization.[6,7] A great deal of research work has been carried out to improve the efficiency. For example, new dyes with the light absorption range extended to the near-infrared and new electrolytes with lower redox potential for higher open-circuit voltage have been developed. As a result, the power-conversion efficiency of DSSC is expected to exceed 15% in the near future.[8] Coupling the DSSCs with photonic crystals (PCs) is a powerful method to enhance the light harvesting. The most commonly used PC structures are SiO_2/TiO_2 multilayers[9,10] and TiO_2 inverse opal layers.[11−13] Míguez's group presented theoretical analysis on the performance of these PC-based DSSCs and attributed the enhanced light harvesting mainly to the mirror behavior of the PC layer, which causes light localization in the absorbing layer (nanocrystalline TiO_2 layer) for frequencies within the stop band range.[4,14] The enhancement effect strongly depends on the position and the width of the stop band of the PC used, which are the key parameters to be considered in the design and optimization of PC-based DSSCs.[15,16] However, those conventional PC structures have some inherent drawbacks, such as clogging channels formed at the interface and the photonic bandgap of the inverse opal layer being unable to be freely tuned for the optimization of light harvesting. Very recently, by using polymeric porogen mixed with the precursor suspensions for stacking of TiO_2 and SiO_2 layers, further optimized nanoparticle-based 1D PCs with enhanced porosity can be achieved, which results in improved mass transport.[17,18] Compared to the conventional DSSCs with thickness around 10 μm, however, the fill factor is still slightly lower, probably due to the electrolyte diffusion being still hindered to some extent.[17]

A novel PC structure, TiO_2 nanotube (NT) PC, has recently been developed and applied to DSSCs.[19−21] This PC structure is actually TiO_2 nanotubes with periodicities along the axial direction of NTs fabricated by the periodic current pulse anodization process. The TiO_2 NT PCs can avoid all of the above-mentioned drawbacks and have been experimentally proven to significantly enhance the efficiency of DSSCs. An added value of the TiO_2 NT PC is that it also works as an absorbing layer, and moreover, it has much slower electron–hole recombination[22−24] as compared with the TiO_2 nanoparticle-based absorbing layer.

To better understand the mechanism of light-harvesting enhancement and to provide guidance for further improvement

Received: September 10, 2013
Accepted: December 6, 2013
Published: December 6, 2013

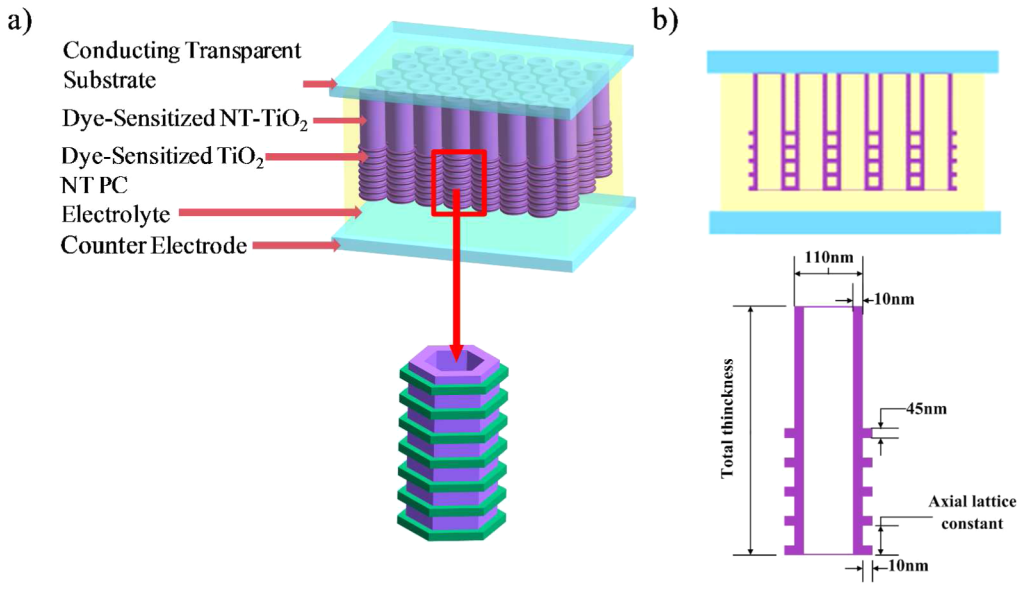

Figure 1. Schematics of the TiO_2 NT-based DSSCs coupled to a NT PC layer: (a) 3D model and (b) cross-sectional view with detailed structural parameters.

in the power conversion efficiency of the DSSCs coupled with TiO_2 NT PCs, a detailed theoretical study is conducted. It is found that the TiO_2 NT PC layer functions as a Bragg mirror and generates Fabry–Perot cavity behavior in the absorbing layer, leading to a significant enhancement in light harvesting for photons with energy in the photonic bandgap and at the band edges. It is also demonstrated that varying the axial lattice constant of the PC layer and diameter of the NTs can effectively tune the optical properties of the photoanode and maximize the photocurrent. A considerable increase in the efficiency of DSSCs beyond 30% can be achieved in the optimized structure. The performance of PC-based DSSCs is also evaluated under different incident angles.

THEORETICAL METHODS

Figure 1 shows the configuration of a PC-coupled TiO_2 NT-based DSSC used in theoretical simulation. The NTs in both layers are arranged in a hexagonal lattice with the geometry similar to the experimental samples. Specifically, the outer diameter and the wall thickness of the NTs are 110 and 10 nm, respectively. The width and thickness of the loops surrounding the NT are 10 and 45 nm, respectively. The total thickness of the NT and PC layers is fixed at 10 μm. The details for the fabrication of the absorbing TiO_2 NT layer and the TiO_2 NT PC layer as well as the assembling of the DSSC can be found from our previous work.[19] Both layers are sensitized by ruthenium dye N719 and infiltrated with liquid redox electrolyte.

In our simulation model, light first passes through the conductive transparent substrate (refractive index $n_{substrate}$ = 1.45) and then reaches the TiO_2 NT layer and subsequently the TiO_2 NT PC layer with the refractive index n_{TiO2} = 2.51. The absorption coefficient of the ruthenium dye, which is represented by the frequency-dependent imaginary part of the refractive index, is obtained by fitting the photocurrent and the absorptance spectra of similar layer and device. Similar to the treatment in ref 4, the electrolyte with refractive index $n_{electrolyte}$ = 1.403, corresponding to propionitrile electrolyte, is the last layer to be modeled in our system, which also fills all the internal space of the NT array. The thickness of substrate and that of the electrolyte layer between PC and counter electrode are set to 10 μm.

The reflection spectra and optical responses are simulated using the finite element method (FEM, Ansoft HFSS) in a 3D model without considering the presence of disorders or defects in both TiO_2 NT PC and TiO_2 NT absorbing layers. To see clearly the optical effect of a PC, the reflectance spectrum of the NT PC layer is obtained by assuming that it is immersed in electrolyte, while the absorption of dye is neglected for clarity.

For the theoretical estimation of the photocurrent enhancement, the light-harvesting efficiency (LHE) is defined as the fraction of incident light intensity (I_0) absorbed by the dye in the DSSCs[4,15]

$$\mathrm{LHE} = A = I_A/I_0 \tag{1}$$

where A is absorptance and I_A is the absorbed light intensity. The incident photon-to-current conversion efficiency (IPCE) can be calculated by the following equation[16]

$$\mathrm{IPCE} = (\mathrm{LHE})\varphi\eta = A\varphi\eta \tag{2}$$

where φ is the quantum yield of charge injection and η is the charge-collecting efficiency by the photoanode. The short-circuit current J_{sc} can then be determined by integrating the product of IPCE and the spectral photon flux incident on the cell[4]

$$J_{sc} = \int q\mathrm{IPCE}(\lambda)F(\lambda)\mathrm{d}\lambda = \int q\mathrm{LHE}(\lambda)\varphi(\lambda)\eta(\lambda)F(\lambda)\mathrm{d}\lambda \tag{3}$$

where q is the electron charge and $F(\lambda)$ is the photon flux as a function of wavelength λ, which is calculated from a standard AM1.5G solar spectral irradiance.[25] Since, in our study, $\varphi(\lambda)$ and $\eta(\lambda)$ are only weakly dependent on the wavelength λ, they are assumed to be constant thoughout our calculations. Thus, by comparing the absorptance of the TiO_2 NT PC-based DSSCs [LHE_{pc}] to the TiO_2 NT-based reference cell [LHE_{ref}], where the smooth NTs are of the same diameter and total length (10 μm) as those of the NT PC, the enhancement in short-circuit photocurrent efficiency ΔJ_{sc} can be estimated using[15]

$$\Delta J_{sc} = \frac{\int[\mathrm{LHE}_{pc}(\lambda)]F(\lambda)\mathrm{d}\lambda - \int[\mathrm{LHE}_{ref}(\lambda)]F(\lambda)\mathrm{d}\lambda}{\int[\mathrm{LHE}_{ref}(\lambda)]F(\lambda)\mathrm{d}\lambda} \tag{4}$$

RESULTS AND DISCUSSION

Figure 2 displays the simulated photonic band structure, the optical reflectance, and absorptance spectra of the TiO_2 NT PC layer with an axial lattice parameter of 150 nm. It can be seen clearly that the TiO_2 NT PC possesses a band gap located at 498–555 nm along the axial direction of NTs (A-Γ direction), and a reflection peak also appears at this wavelength range

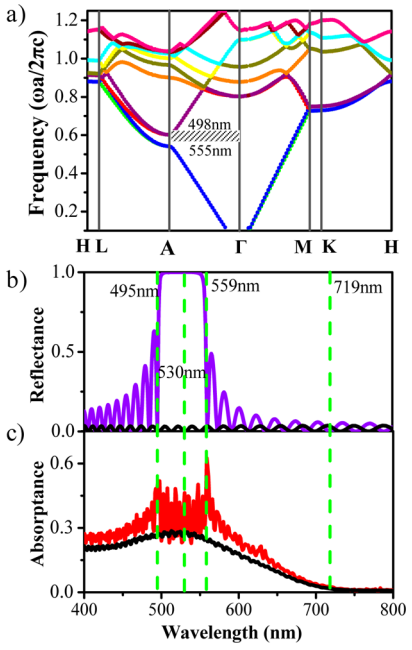

Figure 2. (a) Photonic band structure of TiO_2 NT PC with an axial lattice constant of 150 nm and thickness of 4.5 μm. The shaded region represents the band gap along the A-Γ direction. (b) Reflectance and (c) absorptance of the TiO_2 NT PC layer infiltrated with electrolyte and related DSSC, respectively. For comparison, reflectance and absorptance of a reference layer with smooth NT structure are also plotted as black lines. The green lines indicate the locations of some specific wavelengths as will be discussed below.

because there are no allowed modes in the PC structure. In Figure 2c, a series of sharp increases in absorptance are found to occur in the whole stop band and the band edges.

To study the effect of TiO_2 NT PC on the absorption enhancement of DSSCs, the surface distributions of the electric field amplitude are plotted in Figure 3 for four selected wavelengths: inside the stop band (530 nm), at the edges of the stop band (559 and 495 nm), and far away from the stop band (719 nm), as indicated in green lines in Figure 2. The absorption enhancement effect can be understood in terms of the wavelength-dependent electric field distribution in the NT PC and the NT absorbing layers. Compared with the electric field distribution at long wavelength (Figure 3e), the increased absorbance in the stop band range due to the coupling of the TiO_2 NT PC results from the strong electric field localization in the TiO_2 NT absorbing layer and a thin region of the PC layer close to the interface (Figure 3c). This strong field confinement is caused by the mirror behavior of the NT PC layer, which reflects the waves in the stop band back to the absorbing NT layer.

Strong absorptions can also be observed at the two band edges. As can be seen from Figure 3b and 3d, a huge field envelope is developed inside the entire NT PC layer, a Fabry–Perot cavity like behavior observed in many PC structures.[26] As a result, the optical absorption of the NT PC layer is enhanced. Moreover, for photons at the red edge of the stop band (top of the valence band), the electric field maxima are mostly located at the high refractive index parts (the place of tube with protruding rings, gray regions in Figure 3a) of the NT PC layer, which may result in stronger light absorption. By comparison, at the blue edge (bottom of conduction band), the field maxima are shifted to the low refractive index parts (the place of tube without rings, white regions in Figure 3a).

It is worth noting that in our TiO_2 NT PC coupled DSSC the optical absorption is remarkably enhanced not only within the stop band but also at the edges of the stop band (Figure 2c). This absorption enhancement can be easily understood from the electric field distribution shown in Figure 3b and 3d, where strong electric field penetrates into the NT PC layer, and hence the NT PC layer also contributes to the light harvesting. This effect should be more significant, taking into consideration the larger surface area in the NT PC layer as compared to the PC layer due to the protruding loops surrounding the wall of NTs in the NT PC layer. This is different from the case in the SiO_2/TiO_2 alternate layer or TiO_2 inverse opal layer coupled DSSCs, where the absorption enhancement at the edges of the stop band does not exist or is negligible. Moreover, since the NT PC layer also contributes to the light conversion, this allows us to design and optimize the thickness ratio between the NT PC layer and the NT layer by keeping the total thickness of the photoanode fixed (which will be discussed in a later part of this text). This is also a very important factor to consider in the design of a photoanode since too thick a photoanode will suffer low electron collection efficiency, poor fill factor, and thus low power conversion efficiency.

Apart from the appreciable absorption enhancement observed for photons in and near the stop band, absorptance for photons outside the band gap is also increased (Figure 2c) as a result of increased amount of surface-anchored dye due to the larger surface area in the NT PC layer as compared to the NT layer. The result is consistent with the many experimental observations in bamboo-like TiO_2 NTs, which provide larger surface area as compared to smooth NTs, due both to protruding rings surrounding the NTs and to enlarged spacing between the NTs.[27−29] To understand the "pure" optical effect of NT PC on the enhanced light harvesting in the photoanode, a purely optical enhancement in photocurrent efficiency, O-ΔJ_{sc}, was calculated by subtracting the additional contribution from the increased surface area, which is estimated by the relative surface area increase, $\Delta S = (S_{NT/NT\ PC} - S_{ref})/S_{ref}$, in the model, and it was compared to the overall enhancement in photocurrent efficiency, ΔJ_{sc}, as determined by eq 4.

It has been reported that the photonic lattice constant determines the position of Bragg reflectance peak and thus the photocurrent amplification effects.[14] To better understand the effect of lattice constant on the photocurrent enhancement, the reflectance spectra of the TiO_2 NT PC layer and the absorptance spectra of the corresponding assembled cells are also simulated. As shown in Figure 4a, the reflectance spectra show a red-shift with increasing axial lattice constant; i.e., by increasing the lattice parameter from 110 to 210 nm, the Bragg reflectance peak sweeps from less than 400 to 730 nm, covering almost the whole visible range. Besides the peak position, the width of the stop band slightly increases, while the peak intensity slightly decreases with increasing lattice constant, mainly due to the reduced number of unit cells in a NT PC layer with fixed thickness. Practically, the tuning of the position and width of the Bragg peak can be easily achieved through the tuning of lattice constant by a current pulse anodization process.[16,20] Figure 4b–d presents the calculated absorptance spectra of DSSCs coupled with the NT PC of different axial lattice constant 130, 170, and 210 nm, respectively, showing the strong influence of lattice constant on the spectral range for enhanced light harvesting. The O-ΔJ_{sc} and ΔJ_{sc} attained for

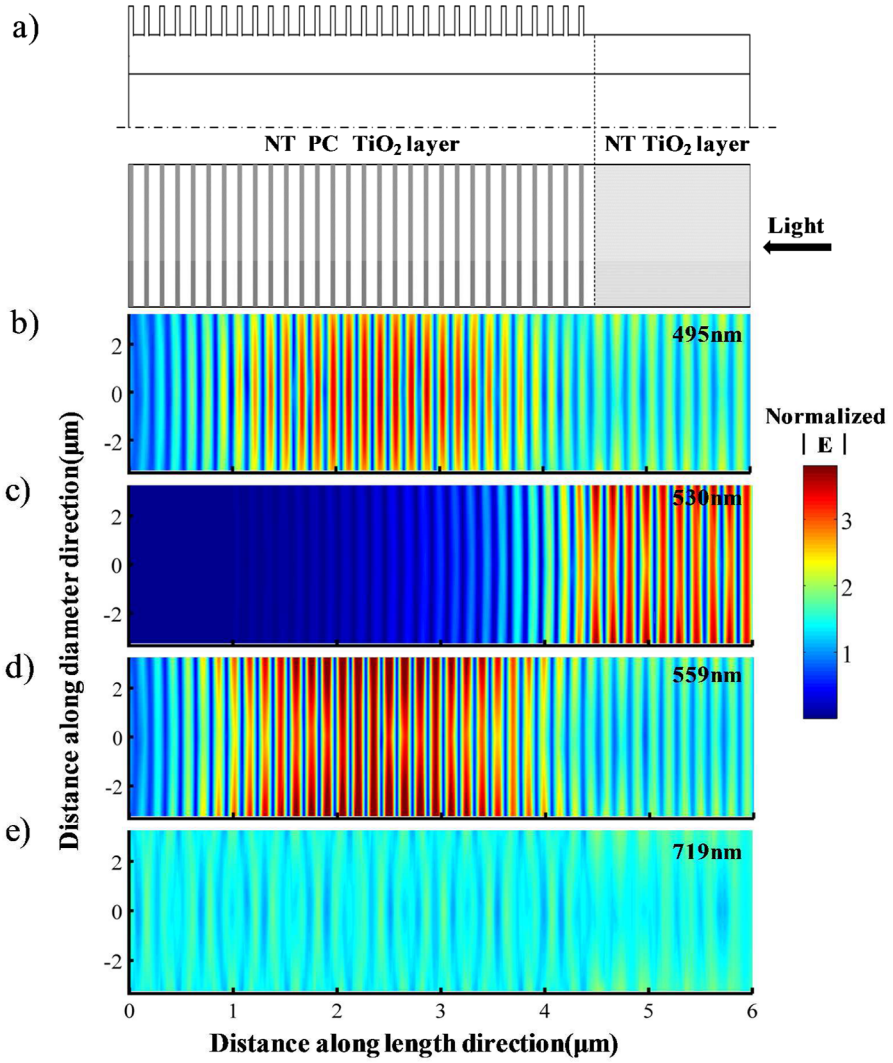

Figure 3. (a) Structure of the TiO_2 NT PC photoanode (lattice constant = 150 nm) used for the electric field calculations. (b–e) 2D surface distribution of the amplitude of the electric field of the TiO_2 NT PC photoanode at four selected wavelengths: (b) 495; (c) 530; (d) 559; and (e) 719 nm.

cells coupled with TiO_2 NT PC with diverse axial lattice constants, whose reflectance spectra are plotted in Figure 4a, are shown in Figure 4e. It can be seen that ΔJ_{sc} strongly depends on the matching of the Bragg peak position of the NT PC and the absorption peak position of the dye. Consequently, the maximum ΔJ_{sc} is obtained when the NT PC has a lattice constant of 150 nm, whose reflectance peak (about 530 nm) significantly overlaps with the dye absorption peak.

Since both the TiO_2 NT PC and NT layers contribute to the light harvesting, there must exist an optimum thickness ratio between the two layers. Keeping the total thickness of the two layers fixed at 10 μm, we calculated the absorption spectra and photocurrent efficiency enhancement of the TiO_2 NT PC coupled DSSCs with different thickness ratios. As can be seen from Figure 5, when the TiO_2 NT PC layer is very thin, the absorption amplification at the edges of the stop band is almost invisible (Figure 5a), while it becomes stronger with increasing thickness of the NT PC layer. On the contrary, as the NT PC layer thickness is increased, the NT layer thickness is decreased, and the absorption enhancement in the stop band becomes weaker and finally becomes even smaller than that of the reference cell (Figure 5c). This is due to the fact that almost all the photons in the stop band are now confined to the NT layer, and a thinner NT layer results in less photon absorption. However, the overall ΔJ_{sc} value remains positive over the entire thickness range of the NT PC layer. This is contributed by a combination of three photocurrent enhancement effects: (1) enhanced stop band absorption in the NT layer, (2) enhanced band edge absorption in the NT PC layer, and (3) enhanced absorption due to increased surface area of the NT PC layer. The maximum of ΔJ_{sc} (29%) is obtained when the NT PC layer has a thickness of 2.25 μm.

Figure 6a displays the calculated reflectance spectra of TiO_2 NT PC layers with different diameters of NTs, which can be easily modified and determined by the anodization voltage in practice.[30] Interestingly, the position and width of the Bragg peak show a noticeable change with the diameter of NTs, which provide further opportunities in the design and optimization of NT PC-based DSSCs via fine tuning of the nanostructures. In particular, when the tubular diameter decreases from 190 to 70 nm, the Bragg reflection peak red-shifts from 495 to 555 nm, and the width of the stop band is dramatically broadened by ~2 times. This is believed to result from the increased effective refractive index in the NT PC layer, and it implies that both the

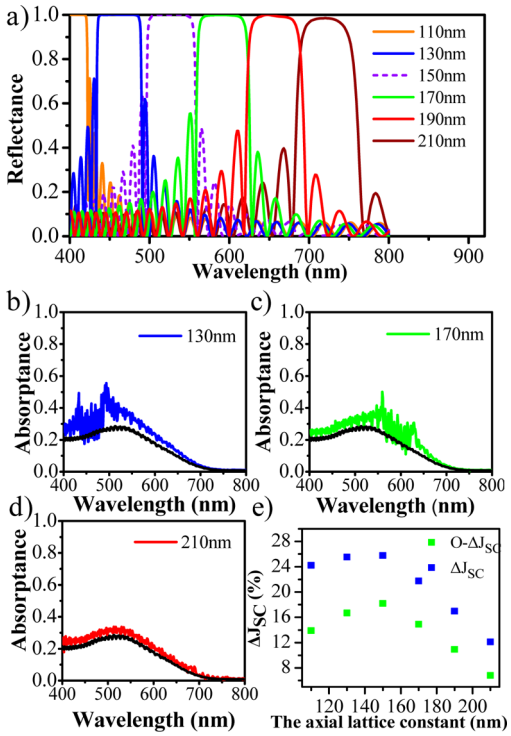

Figure 4. (a) Calculated reflectance spectra of TiO_2 NT PC layers (thickness fixed at 4.5 μm) with different axial lattice constants and (b–d) absorptance spectra of related DSSCs. The black lines in (b–d) are the calculated absorptance spectra of the reference DSSC having the same photoanode thickness. (e) Photocurrent efficiency enhancement versus the axial lattice constant.

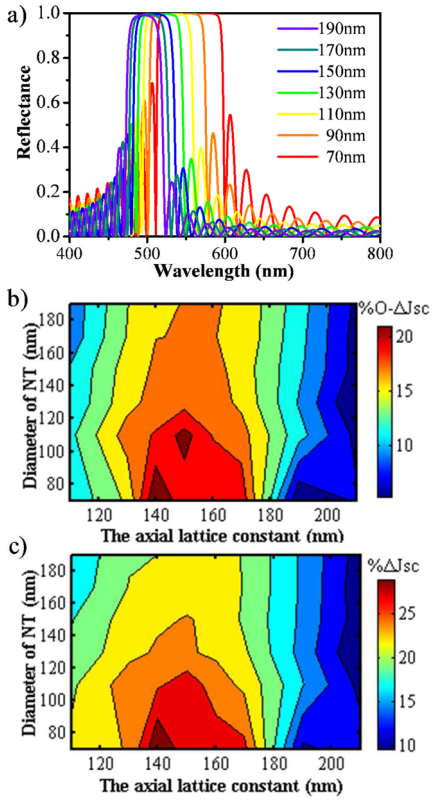

Figure 6. (a) Calculated reflectance spectra of TiO_2 NT PC layers with different diameters of NTs. The axial lattice constant is fixed at 150 nm. (b) Photocurrent enhancement (O-ΔJ_{sc} and ΔJ_{sc}) map for TiO_2 NT PC-based DSSCs with respect to axial lattice constant and NT diameter. The thickness of the TiO_2 NT PC layer and that of the photoanode are fixed at 3.75 and 10 μm, respectively.

axial lattice constant of PC and the lateral diameter of the NTs will affect the performance of the NT PC-based DSSCs. To visualize how they affect the DSSC performance, two-dimensional contours of O-ΔJ_{sc} and ΔJ_{sc} against these structural parameters are plotted, as shown in Figure 6b and 6c, respectively. It can be seen that, in general, the photocurrent enhancement, no matter O-ΔJ_{sc} or ΔJ_{sc}, is more sensitive to the axial lattice parameter than to the NT diameter, with the optimum lattice constant around 140–150 nm. The photocurrent enhancement becomes quite sensitive to the NT diameter only when the lattice parameter is within 130–175 nm, where the Bragg reflection peak of the NT PC has the most overlap with the dye absorption range. Within this lattice parameter range, the general trend of photocurrent enhancement is that it decreases with increasing NT diameter, due to the significant narrowing of the Bragg peak and the blue-shift of the peak, which lead to less overlap between the Bragg peak and dye absorption peak. The maximum ΔJ_{sc} (31%) can be found when the axial lattice constant is around 140 nm and the NT diameter is around 70 nm. The theoretically calculated contour maps shown in Figure 6 clearly show the optimum design parameters for fabrication of TiO_2 NT PC-based DSSCs.

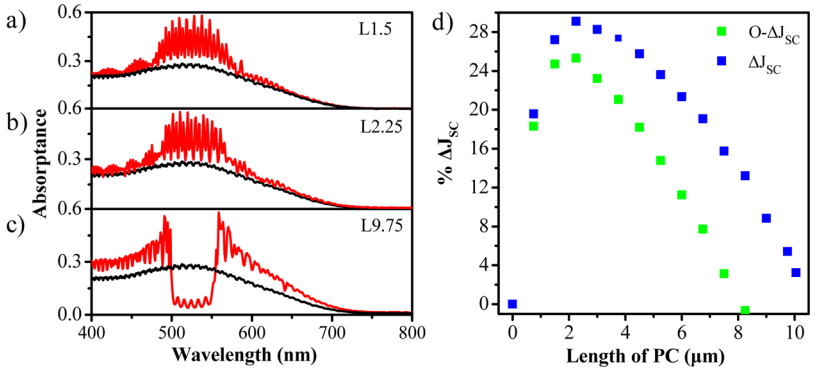

Figure 5. Absorptance spectra of TiO_2 NT PC (lattice constant = 150 nm) based DSSCs with different PC layer thicknesses of (a) 1.5 μm, (b) 2.25 μm, and (c) 9.75 μm. Absorptance of a reference DSSC coupled with smooth NTs and having the same photoanode thickness (10 μm) is shown as black curve. (d) Photocurrent efficiency enhancement versus the thickness of the TiO_2 NT PC layer.

dx.doi.org/10.1021/am4039213 | ACS Appl. Mater. Interfaces 2013, 5, 13022–13028

Finally, the angular dependence of the DSSC performance was studied since, in real applications, the incident angle of solar light keeps on changing. The calculated reflectance spectra of the NT PC layer and the photocurrent efficiency enhancement of the assembled cells under different incident angles (0−75°) are shown in Figure 7. The Bragg peak of the

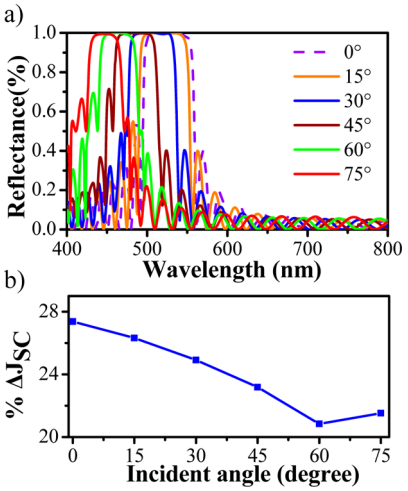

Figure 7. (a) Calculated reflectance spectra of NT PC layer under different incident angles. The thickness and axial lattice constant of the NT PC are 3.75 μm and 150 nm, respectively. (b) Angular dependence of the photocurrent enhancement ΔJ_{sc}. All photoanodes of the cells under study have the same thickness of 10 μm.

TiO_2 NT PC shows a moderate blue-shift from 530 to 450 nm and a gradual narrowing of the peak width as the incident angle increases from 0 to 75°. As a result, the photocurrent enhancement gently decreases by approximately 6% when the incident angle varies from 0 to 60°.

CONCLUSIONS

In this work, the origin of the enhancement of photocurrent efficiency of DSSCs coupled with novel TiO_2 nanotube photonic crystals has been studied. Our analysis indicates that the presence of the TiO_2 NT PC layer will produce both Bragg mirror effect and Fabry−Perot cavity behavior, leading to significant enhancement of light harvesting for photons in the photonic bandgap and at the band edges. Apart from the optical effect of the NT PC, larger surface area in the NT PC layer also enhances the absorption due to the increased amount of surface-anchored dye. A deep insight into the optical response of the nanotube photonic crystal is provided by the calculation of the photonic band structure, reflectance spectrum, and the spatial distribution of the electric field. More importantly, the dependence of DSSC performance on the various structural parameters of the NT PC layer and the light incident angle were calculated, which will provide practical guidance to the design and optimization of PC-based DSSCs. It is believed that optical features of this novel nanotube photonic crystal and the multifunctionalities of TiO_2 will stimulate intensive research of TiO_2 NT PC for applications not only in DSSCs but also in other related fields, such as photocatalysis, water splitting, and so on. In addition, the current theoretical study only takes the enhanced light absorption into consideration. A more comprehensive model, including the electron and electrolyte diffusion in the nanostructured photoanode,[31] is needed in the future to give a more precise description on the photonic crystal coupled photoanode.

AUTHOR INFORMATION

Corresponding Author

*E-mail: aphhuang@polyu.edu.hk.

Notes

The authors declare no competing financial interest.

ACKNOWLEDGMENTS

The work was supported by grants received from the Research Grants Council of the Hong Kong Special Administrative Region (Project Nos. PolyU5163/12E and PolyU5159/13E) and the Hong Kong Polytechnic University (Project Nos. RT5W and 5-ZG91). It was also supported by the municipal government of Guangzhou (Project Nos. 2012A090300013 and 2011J5100001). M.G. and Z.H.Y. thank Dr. L.X. He for help in the theoretical calculation.

REFERENCES

(1) O'Regan, B.; Grätzel, M. *Nature* **1991**, *353*, 737−740.
(2) Hagfeldt, A.; Boschloo, G.; Sun, L.; Kloo, L.; Pettersson, H. *Chem. Rev.* **2010**, *110*, 6595−6663.
(3) Halme, J.; Vahermaa, P.; Miettunen, K.; Lund, P. *Adv. Mater.* **2010**, *22*, E210−E234.
(4) Mihi, A.; Míguez, H. *J. Phys. Chem. B* **2005**, *109*, 15968−15976.
(5) Yella, A.; Lee, H.-W.; Tsao, H. N.; Yi, C.; Chandiran, A. K.; Nazeeruddin, M. K.; Diau, E. W.-G.; Yeh, C.-Y.; Zakeeruddin, S. M.; Grätzel, M. *Science* **2011**, *334*, 629−634.
(6) Grätzel, M. *Acc. Chem. Res.* **2009**, *42*, 1788−1798.
(7) Yu, M.; Long, Y. Z.; Sun, B.; Fan, Z. *Nanoscale* **2012**, *4*, 2783−2796.
(8) Hardin, B. E.; Snaith, H. J.; McGehee, M. D. *Nature Photon.* **2012**, *6*, 162−169.
(9) Colonna, D.; Colodrero, S.; Lindstrom, H.; Di Carlo, A.; Míguez, H. *Energy Environ. Sci.* **2012**, *5*, 8238−8243.
(10) Colodrero, S.; Mihi, A.; Häggman, L.; Ocaña, M.; Boschloo, G.; Hagfeldt, A.; Míguez, H. *Adv. Mater.* **2009**, *21*, 764−770.
(11) Nishimura, S.; Abrams, N.; Lewis, B. A.; Halaoui, L. I.; Mallouk, T. E.; Benkstein, K. D.; van de Lagemaat, J.; Frank, A. J. *J. Am. Chem. Soc.* **2003**, *125*, 6306−6310.
(12) Mihi, A.; Zhang, C.; Braun, P. V. *Angew. Chem., Int. Ed.* **2011**, *50*, 5712−5715.
(13) Kwak, E. S.; Lee, W.; Park, N.-G.; Kim, J.; Lee, H. *Adv. Funct. Mater.* **2009**, *19*, 1093−1099.
(14) Lozano, G.; Colodrero, S.; Caulier, O.; Calvo, M. E.; Míguez, H. n. *J. Phys. Chem. C* **2010**, *114*, 3681−3687.
(15) Mihi, A.; López-Alcaraz, F. J.; Míguez, H. *Appl. Phys. Lett.* **2006**, *88*, 193110.
(16) Tao, C.-a.; Zhu, W.; An, Q.; Li, G. *J. Phys. Chem. C* **2010**, *114*, 10641−10647.
(17) Colodrero, S.; Forneli, A.; López- López, C.; Pellejà, L.; Míguez, H.; Palomares, E. *Adv. Funct. Mater.* **2012**, *22*, 1303−1310.
(18) López- López, C.; Colodrero, S.; Raga, S. R.; Lindstrom, H.; Fabregat-Santiago, F.; Bisquert, J.; Míguez, H. *J. Mater. Chem.* **2012**, *22*, 1751−1757.
(19) Yip, C. T.; Huang, H.; Zhou, L.; Xie, K.; Wang, Y.; Feng, T.; Li, J.; Tam, W. Y. *Adv. Mater.* **2011**, *23*, 5623−5623.
(20) Lin, J.; Liu, K.; Chen, X. *Small* **2011**, *7*, 1784−1789.
(21) Guo, M.; Xie, K.; Lin, J.; Yong, Z.; Yip, C. T.; Zhou, L.; Wang, Y.; Huang, H. *Energy Environ. Sci.* **2012**, *5*, 9881−9888.
(22) Zhu, K.; Neale, N. R.; Miedaner, A.; Frank, A. J. *Nano Lett.* **2006**, *7*, 69−74.
(23) Poudel, P.; Qiao, Q. *Nanoscale* **2012**, *4*, 2826−2838.
(24) Lin, J.; Guo, M.; Yip, C. T.; Lu, W.; Zhang, G.; Liu, X.; Zhou, L.; Chen, X.; Huang, H. *Adv. Funct. Mater.* **2013**, DOI: 10.1002/adfm.201301066.

(25) Spandard spectrum taken from http://www.nrel.gov/rredc. (Accessed January 15, 2013).
(26) Kozina, O. N.; Mel'nikov, L. A. *Laser Phys.* **2004**, *14*, 727−732.
(27) Kim, D.; Ghicov, A.; Albu, S. P.; Schmuki, P. *J. Am. Chem. Soc.* **2008**, *130*, 16454−16455.
(28) Xie, Y.-L.; Li, Z.-X.; Xu, H.; Xie, K.-F.; Xu, Z.-G.; Zhang, H.-L. *Electrochem. Commun.* **2012**, *17*, 34−37.
(29) Roy, P.; Kim, D.; Lee, K.; Spiecker, E.; Schmuki, P. *Nanoscale* **2010**, *2*, 45−59.
(30) Roy, P.; Berger, S.; Schmuki, P. *Angew. Chem., Int. Ed.* **2011**, *50*, 2904−2939.
(31) Gálvez, F. E.; Kemppainen, E.; Míguez, H.; Halme, J. *J. Phys. Chem. C* **2012**, *116*, 11426−11433.